

Quantification of PpIX concentration in basal cell carcinoma and squamous cell carcinoma models using spatial frequency domain imaging

Ulas Sunar,^{1,*} Daniel J. Rohrbach,¹ Janet Morgan,² Natalie Zeitouni,² and Barbara W. Henderson¹

¹Department of Cell Stress Biology & PDT Center, Roswell Park Cancer Institute, Buffalo, NY 14263, USA

²Department of Dermatology, Roswell Park Cancer Institute, Buffalo, NY 14263, USA

*ulas.sunar@roswellpark.org

Abstract: 5-aminolaevulinic acid photodynamic therapy (ALA-PDT) is an attractive treatment option for nonmelanoma skin tumors, especially for multiple lesions and large areas. The efficacy of ALA-PDT is highly dependent on the photosensitizer (PS) concentration present in the tumor. Thus it is desirable to quantify PS concentration and distribution, preferably noninvasively to determine potential outcome. Here we quantified protoporphyrin IX (PpIX) distribution induced by topical and intra-tumoral (it) administration of the prodrug ALA in basal and squamous cell carcinoma murine models by using spatial frequency domain imaging (SFDI). The *in vivo* measurements were validated by analysis of the *ex vivo* extraction of PpIX. The study demonstrates the feasibility of non-invasive quantification of PpIX distributions in skin tumors.

©2013 Optical Society of America

OCIS codes: (170.0170) Medical optics and biotechnology; (170.5180) Photodynamic therapy; (170.3880) Medical and biological imaging; (170.1610) Clinical applications.

References and links

1. T. M. Busch, S. M. Hahn, E. P. Wileyto, C. J. Koch, D. L. Fraker, P. Zhang, M. Putt, K. Gleason, D. B. Shin, M. J. Emanuele, K. Jenkins, E. Glatstein, and S. M. Evans, "Hypoxia and Photofrin uptake in the intraperitoneal carcinomatosis and sarcomatosis of photodynamic therapy patients," *Clin. Cancer Res.* **10**(14), 4630–4638 (2004).
2. X. Zhou, B. W. Pogue, B. Chen, E. Demidenko, R. Joshi, J. Hoopes, and T. Hasan, "Pretreatment photosensitizer dosimetry reduces variation in tumor response," *Int. J. Radiat. Oncol. Biol. Phys.* **64**(4), 1211–1220 (2006).
3. A. Bogaards, H. J. Sterenberg, J. Trachtenberg, B. C. Wilson, and L. Lilge, "In vivo quantification of fluorescent molecular markers in real-time by ratio imaging for diagnostic screening and image-guided surgery," *Lasers Surg. Med.* **39**(7), 605–613 (2007).
4. E. H. Moriyama, A. Kim, A. Bogaards, L. Lilge, and B. Wilson, "A ratiometric fluorescence imaging system for surgical guidance," *Adv. Opt. Technol.* **2008**, 532368 (2008).
5. R. B. Saager, D. J. Cuccia, S. Saggese, K. M. Kelly, and A. J. Durkin, "Quantitative fluorescence imaging of protoporphyrin IX through determination of tissue optical properties in the spatial frequency domain," *J. Biomed. Opt.* **16**(12), 126013 (2011).
6. A. E. Oro, K. M. Higgins, Z. Hu, J. M. Bonifas, E. H. Epstein, Jr., and M. P. Scott, "Basal cell carcinomas in mice overexpressing sonic hedgehog," *Science* **276**(5313), 817–821 (1997).
7. M. Grachtchouk, R. Mo, S. Yu, X. Zhang, H. Sasaki, C. C. Hui, and A. A. Dlugosz, "Basal cell carcinomas in mice overexpressing Gli2 in skin," *Nat. Genet.* **24**(3), 216–217 (2000).
8. T. L. Becker, "Irradiance: A parameter determining oxygenation during topical photodynamic therapy (PDT)" (University at Buffalo, SUNY, Buffalo, 2010).
9. C. M. Gardner, S. L. Jacques, and A. J. Welch, "Fluorescence spectroscopy of tissue: recovery of intrinsic fluorescence from measured fluorescence," *Appl. Opt.* **35**(10), 1780–1792 (1996).
10. D. J. Cuccia, F. Bevilacqua, A. J. Durkin, F. R. Ayers, and B. J. Tromberg, "Quantitation and mapping of tissue optical properties using modulated imaging," *J. Biomed. Opt.* **14**(2), 024012 (2009).
11. C. W. Chin, A. J. Foss, A. Stevens, and J. Lowe, "Differences in the vascular patterns of basal and squamous cell skin carcinomas explain their differences in clinical behaviour," *J. Pathol.* **200**(3), 308–313 (2003).

12. R. B. Saager, A. Truong, D. J. Cuccia, and A. J. Durkin, "Method for depth-resolved quantitation of optical properties in layered media using spatially modulated quantitative spectroscopy," *J. Biomed. Opt.* **16**(7), 077002 (2011).
-

1. Introduction

Nonmelanoma skin cancer (basal cell carcinoma (BCC) and squamous cell carcinoma (SCC)) is the most frequently diagnosed human cancer. Photodynamic therapy using 5-aminolevulinic acid (ALA-PDT) is an attractive alternative treatment option for nonmelanoma skin cancer in situations where surgery is suboptimal, for example due to a large number of tumors or tumors located in sensitive areas such as the face. For effective PDT, a sufficient amount of photosensitizer (PS) needs to accumulate in tumors. In most clinical studies, PS accumulation in each tumor is assumed to be the same for a given administered dose. However, PS distribution in tissue can show significant inter and intra-patient heterogeneity [1]. Insufficient local PS concentration can lead to suboptimal PDT dose and thus treatment failure. Therefore there is considerable motivation for assessing the *in vivo* PS distribution prior to treatment light activation, so that light dose might be adjusted accordingly [2].

Fluorescence spectroscopy is frequently used for quantification of the ALA-induced protoporphyrin IX (PpIX) content, since the fluorescence contrast is usually higher than the absorption contrast *in vivo*. Spectroscopic measurements, however, do not give information about PpIX distribution. Moreover, fluorescence signal is affected by the tissue optical properties, and thus is not directly related to PpIX concentration. Ratiometric methods (with respect to optical attenuation and/or autofluorescence) partially correct this signal distortion [3,4]. Recently spatial frequency domain imaging (SFDI) technique has been proposed for quantification of absolute fluorescence concentration by eliminating the variations in fluorescence signal due to absorption and scattering at both excitation and emission wavelengths [5].

In this work, we utilized a custom SFDI system for quantifying the absolute PpIX concentration in basal cell carcinoma (BCC) and squamous cell carcinoma (SCC) models, to which ALA was applied topically and intra-tumorally, respectively. PpIX concentration mapping clearly showed the improvement in tumor contrast in SCCs, mainly because SCCs had high intra-tumor optical absorption compared to surrounding normal tissue. Noninvasive imaging results were validated with analysis of the *ex vivo* extraction of PpIX. Thus we conclude that noninvasive SFDI can accurately quantify PpIX concentration distribution noninvasively in nonmelanoma skin tumors.

2. Materials and methods

2.1 Animal and tumor models

All animal experiments followed protocols approved by the IACUC of Roswell Park Cancer Institute (RPCI). Transgenic K5-Gli mice were acquired from Dr. Andrezej Dlugosz at the University of Michigan and bred in our domestic colony. These mice have an activated Sonic hedgehog (Shh) signaling pathway and overexpress the Gli2 downstream transcription factor, which drives proliferation and leads to the development of spontaneous multiple BCC in the skin [6,7]. The spontaneous BCCs are a histologically similar representation of nodular BCCs in human skin [6–8]. BCCs can occur with multiple tumors and over large areas, thus topical application of ALA (20% ALA in a topical vehicle or cream moisture (Kerastick Dusa, Massachusetts)) is the usual clinical option. Two Gli mice from the breeding colony were chosen for imaging once they spontaneously developed BCC tumors on their tails. Both mice were approximately 6 months old and one mouse had two tumors while the other had one. Tumors were selected at the early stage so that tumor sizes were small, ~3 mm in largest dimension and reasonably flat. To reduce the curvature effects of mice tails, a piece of clear plexiglass was placed over the tail so that the top of the tail and matching Intralipid solution surface were kept at the same height. Twenty mg of 5-ALA-hydrochloride (A3785, Sigma)

was dissolved in 80 mg of moisturizing cream (Moistrel) immediately before application to make a 20% ALA solution. This solution was applied to Gli BCCs 4 h prior to imaging for optimal PpIX accumulation and covered with Opsite to keep the cream on the tumor for the entire time. On the other hand, squamous cell carcinoma (SCC) can be locally aggressive and invasive and may be more suitable for interstitial PDT treatment, with ALA applied intravenously (iv) or intratumorally (it). FaDu human epithelial cells derived from a head and neck SCC of the hypopharynx were implanted in SCID mice to serve as an SCC model. Two SCID mice (age 6 months) were implanted subcutaneously on the lower, right flank with 2.5×10^6 FaDu cells. Flank region was chosen due to its relative flatness as well as to minimize breathing artifacts. After 7 days, tumors had grown to ~ 3 mm diameter in size while remaining reasonably flat with negligible thickness. Twenty μL the ALA solution (250 mg/kg of ALA, in 0.4 M sodium acetate) were injected directly into the tumor 1h prior to imaging. Both groups of mice were immobilized during measurements with an inhaled anesthetic mixture of isoflurane and oxygen.

2.2 Custom imaging setup

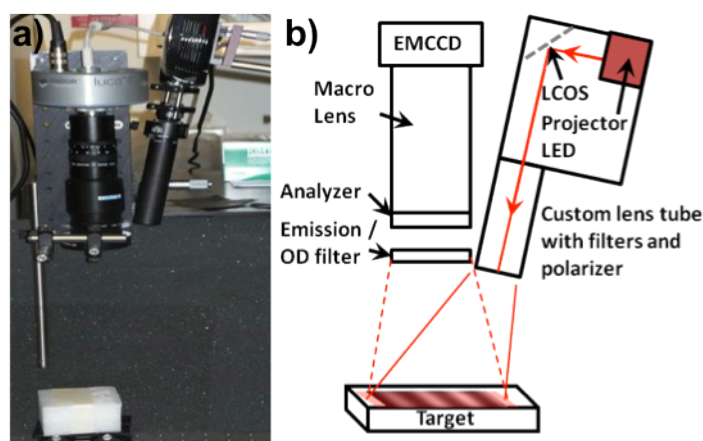


Fig. 1. Diagram and picture of the instrument. The system uses a projector with a built-in red LED, 20 nm band-pass filtered at 635 nm light to project images of varying spatial frequencies onto tissue simulating phantoms or tissue (Target). The reflected light field is captured by an EMCCD camera with adjustable filters to selectively capture emission and excitation light. Crossed linear polarizers reduced specular reflection.

A schematic diagram of the custom spatial frequency domain imaging (SFDI) setup is shown in Fig. 1. The setup consisted of a modified projector (Aaxa Tech.) to spatially modulate the light into the desired frequency and phase pattern. Light from the projector LEDs was directed onto the liquid crystal on silicon (LCOS) chip of the projector where it was spatially modulated to produce the desired pattern (Fig. 1). The tube lens of the projector was removed and replaced with a 100 mm focal length achromatic lens (#AC254-100-A, Thorlabs) for a shorter working distance of 20 cm. The projector contains 3 built-in LEDs (red, green and blue). We used two band-pass filters to select the wavelengths of interest from the full spectrum of the LEDs. The red LED light of the projector was bandpass-filtered at $630 \text{ nm} \pm 10 \text{ nm}$ for imaging PpIX optical properties at the excitation peak as well as PpIX fluorescence. A $660 \text{ nm} \pm 20 \text{ nm}$ band-pass filter was used to quantify optical properties at the emission wavelength of PpIX. The periodic structured illumination pattern with selected frequency and phase images was projected onto the target surface. Reflected light was collected by the lens and focused to the compact Electron Multiplying CCD (EMCCD) camera (Luca, Andor Tech.). Cross-polarizers in front of the projector and camera rejected

specularly reflected light, while a 650 nm long-pass fluorescence filter was used for imaging PpIX fluorescence and an OD filter for reflectance imaging.

To quantify absorption and scattering parameters, 6 spatial frequencies (f) from 0 to 1.7 cm^{-1} and three phases ($0, 2\pi/3, 4\pi/3$) were used. In reflectance and fluorescence imaging modes, EMCCD acquisitions were set at 2s. For optical property quantification, 3 phase and 6 spatial frequency data acquisition time was $\sim 36\text{s}$ ($2\text{s} \times 6 \times 3$) for both the excitation and emission wavelengths. Fluorescence measurement time was 6s since only the continuous wave (CW) frequency (0 cm^{-1}) was acquired. The measurement time could be reduced for fast acquisition schemes by increasing the LED power (currently it is $100 \mu\text{W}/\text{cm}^2$ due to the low power of the LED inside the projector) and by utilizing the EM gain and removing the OD filter.

2.3 Model for fluorescence concentration quantification

PpIX fluorescence concentration was quantified by the Gardner model that corrects raw fluorescence signal by compensating for optical absorption (μ_a) and scattering (μ_s) loss both at excitation and emission wavelengths [5,9]. In this model, the fluorescence correction factor, $X_{1D}(\lambda_{ex}, \lambda_{em})$ is determined by the expression:

$$X_{1D}(\lambda_{ex}, \lambda_{em}) = \frac{C_1(\lambda_{ex})C_3(\lambda_{em})}{k_1(\lambda_{ex})/\delta(\lambda_{ex}) + k_3(\lambda_{em})/\delta(\lambda_{em})} \cdot \frac{C_2(\lambda_{ex})C_3(\lambda_{em})}{k_2(\lambda_{ex})/\delta(\lambda_{ex}) + k_3(\lambda_{em})/\delta(\lambda_{em})} \quad (1)$$

Here X_{1D} represents the effective path-length during excitation light penetrating into and escape of the emitted fluorescence from the tissue, $\delta = 1/[3\mu_a(\mu_a + \mu_s)']^{1/2}$ is the effective penetration depth at the specified wavelength and $C_1, C_2, C_3, k_1, k_2, k_3$ are functions of diffuse reflectance R_d at excitation and emission wavelengths and are determined empirically previously [9]. Bulk optical absorption (μ_a) and scattering (μ_s) parameters were quantified by fitting spatial frequency domain reflectance ($R_d(f)$) data with a modified frequency-domain diffusion model by using a reference phantom with known optical properties by using custom Matlab program [10].

2.4 Ex vivo PpIX analysis

Ex vivo gross quantification of PpIX in tissue samples was performed on solubilized tissue extracts [8]. The tumor and neighboring skin pieces were excised and placed in a tube containing 0.5 mL of SOLVABLE™ (PerkinElmer). PpIX (Sigma) solution was added to control tissue samples solubilized in SOLVABLE™ to obtain a PpIX standard curve. The peak fluorescence in the emission spectrum (Ex 407 nm, Em 620-650 nm) was determined as a measure of PpIX signal in the solution. Protein content was quantified using the Bio-Rad D_C protein assay kit and a protein standard curve was created using bovine serum albumin (BSA) solutions. PpIX fluorescence signal was normalized to protein levels.

3. Results and discussion

3.1 System calibration

The system was characterized with multiple phantoms made by titrating the optical properties. Similarly, fluorescence phantoms were made by titrating the PpIX concentration. Reconstructed raw fluorescence values with respect to concentration were used as a “calibration curve” to obtain absolute PpIX concentrations *in vivo*.

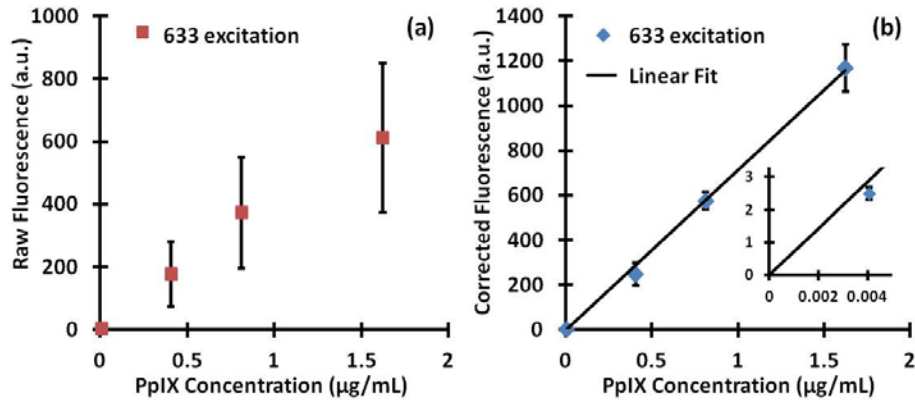


Fig. 2. (a) Uncorrected (raw) PpIX fluorescence (b) Attenuation corrected PpIX fluorescence with respect to concentration using all phantoms at different absorption and scattering parameters. Inset in b) zoom in to the lowest detected PpIX concentration (~ 4 ng/mL). Error bars represent standard deviation of the fluorescence signal due to differences in optical properties.

Figure 2 shows the raw fluorescence intensity with respect to PpIX concentrations (0.4, 0.8, 1.6 $\mu\text{g/mL}$) at different optical parameter ranges of $\mu_a = 0.10$ and 0.50 cm^{-1} and $\mu_s = 10$ and 20 cm^{-1} . The raw fluorescence signal showed great variations with respect to optical parameters, but attenuation corrected fluorescence showed much less variation with respect to PpIX concentration. Our phantom experiments showed that the detection sensitivity of the system is better than 4 ng/mL by utilization of the electron multiplying gain (set at 50) of the EMCCD camera. Higher gain settings and LED power signals can further increase this detection sensitivity.

3.2 *In vivo* imaging

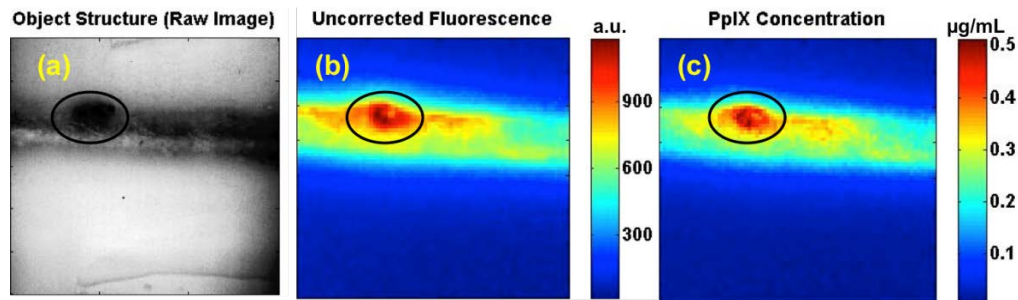


Fig. 3. Representative images of a BCC on the tail of a Gli mouse 4h after topical-ALA administration. (a) Whitelight structural image showing the tumor area and topical ALA application site. (b) Uncorrected PpIX fluorescence image showing the tumor and surrounding application area. (c) PpIX fluorescence concentration indicating higher contrast between the tumor and surrounding area compared to the uncorrected image.

A representative image of a BCC on the tail of a Gli mouse 4 h after topical application of ALA on the tumor and surrounding nearby area is shown in Fig. 3. The uncorrected fluorescence image (Fig. 3(b)) shows a high PpIX signal near the tumor area with some signal coming from normal tail tissue (825 ± 106 a.u. vs. 465 ± 33 a.u. respectively), whereas the corrected PpIX concentration map shows a more localized signal within the tumor and less PpIX in the area near tumor ($0.44 \pm 0.07 \mu\text{g/mL}$ vs. $0.28 \pm 0.03 \mu\text{g/mL}$ respectively). Absolute PpIX concentrations have a maximum value of $\sim 0.5 \mu\text{g/mL}$, and an average value of $\sim 0.35 \mu\text{g/mL}$ in the region of interest of the tumor.

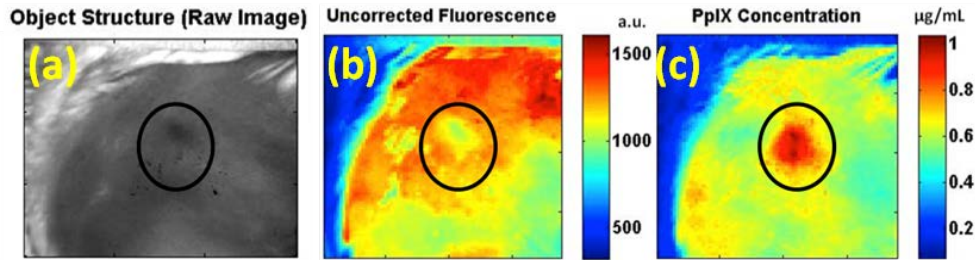


Fig. 4. Representative images of a FaDu tumor 1h after it-administration of ALA. (a) Whitelight structural image showing the tumor area and ALA injection site. (b) The uncorrected fluorescence image does not show localized contrast. (c) PpIX fluorescence concentration indicating higher contrast between the tumor and surrounding area compared to the uncorrected image.

Figure 4 shows representative images of a FaDu tumor in a SCID mouse 1h after it-administration of ALA. Figure 4(a) shows the whitelight image to indicate the tumor location. Tumors were small (~3 mm diameter), thus the thicknesses were assumed to be negligibly small. The uncorrected fluorescence signal (Fig. 4(b)) did not show tumor contrast (1152 ± 72 a.u. vs. 1411 ± 86 a.u. in the tumor and normal respectively), but the absolute PpIX concentration image demonstrated a clear tumor contrast compared to normal surrounding tissue (1.10 ± 0.12 $\mu\text{g/mL}$ vs. 0.76 ± 0.06 $\mu\text{g/mL}$ respectively). As compared to Figs. 3(b) and 3(c), Figs. 4(b) and 4(c) demonstrate clear improvement in tumor contrast provided by the PpIX concentration mapping. This is possibly due to the fact that SCCs are well vascularized, and have high microvessel density within the tumor compared to BCCs, which have even less microvessel density compared to stroma [11]. Indeed, the contrast in optical properties was higher in the FaDu tumor compared to the BCC tumor, as clearly indicated by Table 1. For the FaDu tumor shown in Fig. 4, tumor absorption parameter (μ_a) was ~61% and scattering parameter was ~12% higher than surrounding normal tissue at the excitation wavelength, and ~75% and ~12% higher at the emission wavelength. This optical contrast was not observed in the BCC tumor shown in Fig. 3, where the tumor absorption contrast with respect to skin was virtually the same at both the excitation and emission wavelengths, and scattering parameter was ~8% and ~11% lower in the tumor at the excitation and emission wavelengths, respectively (Table 1).

Table 1. Optical Parameters (μ_a , μ_s) Quantified with SFDI at the Emission (~660 nm) and Excitation (~630 nm) Wavelengths for Tumor and Normal Sites in SCID and Gli Mice^a

Wavelength		SCID		Gli	
		FaDu SCC	normal	BCC	normal
Emission	μ_a	0.35 ± 0.06	0.20 ± 0.01	0.21 ± 0.02	0.22 ± 0.02
	μ_s	9.23 ± 0.99	8.25 ± 0.54	13.21 ± 1.22	14.62 ± 0.70
Excitation	μ_a	0.53 ± 0.07	0.33 ± 0.01	0.33 ± 0.03	0.33 ± 0.02
	μ_s	9.34 ± 0.97	8.32 ± 0.50	13.41 ± 0.63	14.52 ± 0.37

^aValues are given as mean \pm standard deviation.

To compare the noninvasive *in vivo* imaging results with *ex vivo* PpIX analysis, we used a hand-drawing tool function (imfreehand, Matlab) to choose not less than 20×20 pixel region of interest (ROI) for both tumor and normal tissue determined from whitelight and digital photographic pictures. Mean and standard deviation values of each ROI were plotted with respect to the *ex vivo* solubilization analysis as shown in Fig. 5. The correlation of *ex vivo* values with respect to uncorrected raw fluorescence signals had a correlation coefficient of 0.658 ($r^2 = 0.658$), which improved with the corrected fluorescence signal to $r^2 = 0.863$.

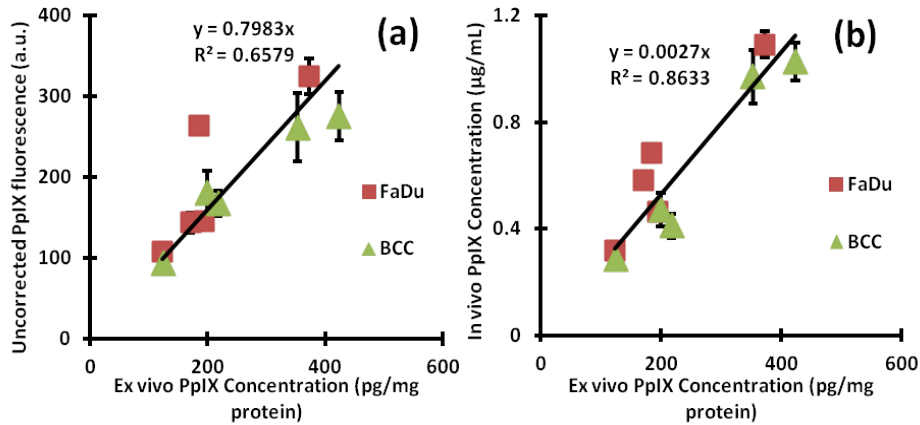


Fig. 5. (a) Uncorrected fluorescence signal vs *ex vivo* PpIX concentration. (b) *In vivo* PpIX concentration vs *ex vivo* PpIX concentration. Linearity increased from 0.658 to 0.863.

Generally, skin layer covers tumor and consideration of skin layer may result in more accurate quantification of the tumor tissue. However, in this study, imaged tumors were small and skin layer effect is assumed to be minimal compared to human skin. Multi-wavelength approach can be helpful to investigate the skin layer, as was demonstrated previously [12]. Since our instrument has very few wavelengths, this approach is not practical for accurate characterization of skin layers. We are updating our current instrument by adding multi-wavelength LED sources and layer effects may be investigated in the future clinical studies.

4. Conclusion

We utilized a custom SFDI system to quantify the absolute concentration of PpIX in BCC and SCC models. PpIX concentration quantification showed more contrast improvement for the case of SCC model with intra-tumoral administration. Noninvasive imaging results were validated by correlation with PpIX values determined by the SOLVABLE™ solubilization of samples from the same tumors imaged *in vivo*. Thus we conclude that SFDI can accurately quantify PpIX concentration distribution noninvasively in nonmelanoma skin tumors.

Acknowledgments

This research is partially supported by RPCI Startup Grant (U. Sunar) and NCI CA55791 (B. W. Henderson). We thank David Bellnier for useful discussions related to solubilization analysis. We thank Soren Konecky, Alexander Lin in Dr. Bruce Tromberg lab and Rolf Saager in Dr. Antony Durkin Lab at University of California Irvine for useful discussions related to SFDI.